

## Supporting Information for

# Aggregation-Induced Visible Light Absorption Makes Reactant 1,2-Diisocyanoarenes Acting as Photosensitizer in Double Radical Isocyanide Insertions

Wenmin Wang,<sup>a,†</sup> Xiaoyang Sun,<sup>b,†</sup> Jian Qu,<sup>c</sup> Xiaoyu Xie,<sup>a</sup> Zheng-Hang Qi,<sup>a</sup> Daocheng Hong,<sup>a</sup> Su Jing,<sup>c</sup> Dong Zheng,<sup>a</sup> Yuxi Tian,<sup>a</sup> Haibo Ma,<sup>a</sup> Shouyun Yu,<sup>\*,b</sup> and Jing Ma<sup>\*,a,b</sup>

<sup>a</sup>Key Laboratory of Mesoscopic Chemistry of MOE School of Chemistry & Chemical Engineering, Nanjing University, Nanjing, 210093, People's Republic of China

<sup>b</sup>State Key Laboratory of Analytical Chemistry for Life Science, Jiangsu Key Laboratory of Advanced Organic Materials, School of Chemistry and Chemical Engineering, Nanjing University, Nanjing 210023, China.

<sup>c</sup>School of Chemistry and Molecular Engineering, Nanjing Tech University, Nanjing 211800, China.

<sup>†</sup> These authors contributed equally to this article.

### List of content

1. Screening of reaction conditions .....	S3
2. The maximum absorption wavelengths and relative energies of isomers.....	S4
3. Details of CASSCF/CASPT2 Calculations .....	S5
4. Comparison between experiment and DFT calculation: IR spectra .....	S10
5. Binding energies of $\pi$ - $\pi$ stacking configuration in crystal.....	S11
6. Experimental and calculated values for $S_0 \rightarrow S_1$ transitions.....	S12
7. The electrostatic potential and monomer charge of $\pi$ - $\pi$ stacking configuration..	S13
8. Natural transition orbitals of $S_0 \rightarrow S_1$ transition.....	S14
9. Computational results using different DFT functionals.....	S15
10. TDDFT calculations on $\pi$ stacking arrays with background charges.....	S18
11. Experimental absorption spectra of unitary, binary and trinary mixtures <b>1</b> , <b>2</b> , <b>Bn<sub>2</sub>NH</b> in CH <sub>3</sub> CN solvent.....	S19
12. TDDFT calculation results using B3LYP/6-311+G(d, p) of monomer @ CH <sub>3</sub> CN and monomer @ Et <sub>2</sub> O solvent and AIMD simulations of solvated <b>1</b> in both CH <sub>3</sub> CN and Et <sub>2</sub> O solvent molecules.....	S20
13. The experimental absorption spectrum of <b>1</b> in other solvents.....	S21

14. The absorption spectra of binary and ternary mixtures of <b>1</b> , <b>2</b> ( <b>7</b> ), and Bn <sub>2</sub> NH (Bn <sub>3</sub> N) in CH <sub>3</sub> CN solvent.....	S22
15. TDDFT and experimental absorption spectra of product <b>3</b> .....	S23
16. The fluorescence quenching of the mixture of <b>1</b> , <b>2</b> and Bn <sub>2</sub> NH.....	S24
17. Frontier molecular orbitals of donors and acceptors in reactions.....	S25
18. The absorption wavelengths and oscillator strengths of the isolated <b>4</b> and embedded <b>4</b> @ BG (n = 3).....	S26

## 1. Screening of reaction conditions

**Table S1. Action Spectrum.**<sup>a,b,c</sup>

Reaction scheme: 1 + C<sub>8</sub>F<sub>17</sub>-I  $\xrightarrow[\text{blue LED, rt}]{\text{Bn}_2\text{NH, CH}_3\text{CN}}$  3

$\lambda(\text{nm})$	401	439	459	481	501	520.5	560.5
W(1/2) (nm)	9.5	8	8	8.5	8	8.5	8
T (%)	73	75	89	86	77	90	94
Yield (%)	11	22	63	31	17	20	0

<sup>a</sup>Reaction conditions: a solution of **1** (0.10 mmol), **2** (0.20 mmol) and Bn<sub>2</sub>NH (0.10 mmol) in CH<sub>3</sub>CN (2.0 mL) was irradiated by blue LED strips for 24 h through narrow and pass filters. <sup>b</sup> $\lambda$ : wavelength; W(1/2): half-peak width; T = transmittance. <sup>c</sup>Isolated yields.

## 2. The maximum absorption wavelengths and relative energies of isomers of 1

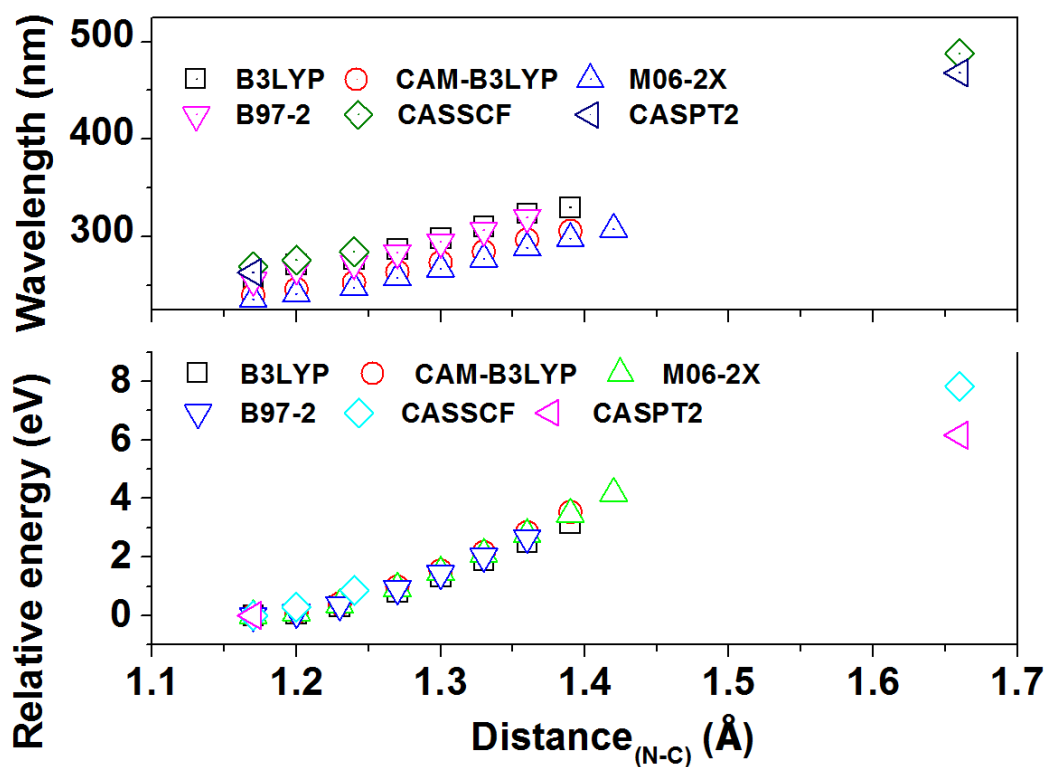


**Figure S1.** The maximum absorption wavelengths and relative energies of isomers of 1 with different N-C distances, obtained at different computational levels.

For the isolated molecule, all the selected computation methods gave similar results, as shown in Figure S1.

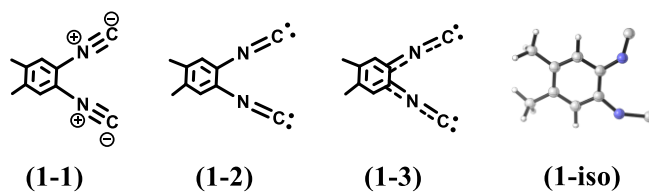
### 3. Details of CASSCF/CASPT2 Calculations

To get excitation energies of low-lying excited states of molecule **1** with different N-C distances,  $r_{\text{N-C}}$ , the state-average complete active space self-consistent field (SA-CASSCF) method was applied to get multiconfigurational wave functions of ground state and some low-lying singlet excited states. Moreover, Multi-state (MS) CASPT2 method was used to correct excitation energies by adding dynamic correlation effect.

In this case, we chose four geometries, which are **(1-1)** with  $r_{\text{C-N}} = 1.17 \text{ \AA}$ , **(1-2)** with  $r_{\text{C-N}} = 1.20 \text{ \AA}$ , **(1-3)** with  $r_{\text{C-N}} = 1.24 \text{ \AA}$  and **(1-iso)** sampling from AIMD simulation. Totally 14 electrons and 14 orbitals (all  $\pi$ -orbitals) were selected for each geometry, and (14,14)CASSCF/PT2 calculation was performed with ANO-L-VDZP basis set using MOLCAS package. For all the studied isomers, symmetry was fixed as  $C_1$ . The number of states for state-average was set as 5, 5, 5 and 3 for **(1-1)**, **(1-2)**, **(1-3)**, and **(1-iso)**, respectively. The multi-state CASPT2 method was used to obtain more accurate excitation energies of **(1-1)** (with 5 states) and **(1-iso)** (with 3 states). Furthermore, RASSI module in MOLCAS was performed to get oscillator strengths of CASSCF states based on dipole transition strengths. **Table S2** shows results of the predominant excitation configurations for lowest singlet excited  $S_1$  of four molecules. And 14 orbitals in active space of the 4 systems are displayed in **Figure S3**.

### 3.1. CASSCF results: CI-weights of S<sub>1</sub>

Table S2: CI-weights of S<sub>1</sub> in (14,14) CASSCF



Species	Configuration <sup>a</sup>	weight
(1-1)	22222121000000	0.36
	22222210100000	0.35
(1-2)	22222211000000	0.36
	22222120100000	0.34
(1-3)	22222210100000	0.34
	22222121000000	0.34
(1-iso)	22222210000100	0.74

<sup>a</sup> The number 2 means double occupation, 1 means single occupation and 0 means non-occupation.

### 3.2. CASSCF results: active orbitals in CASSCF calculations

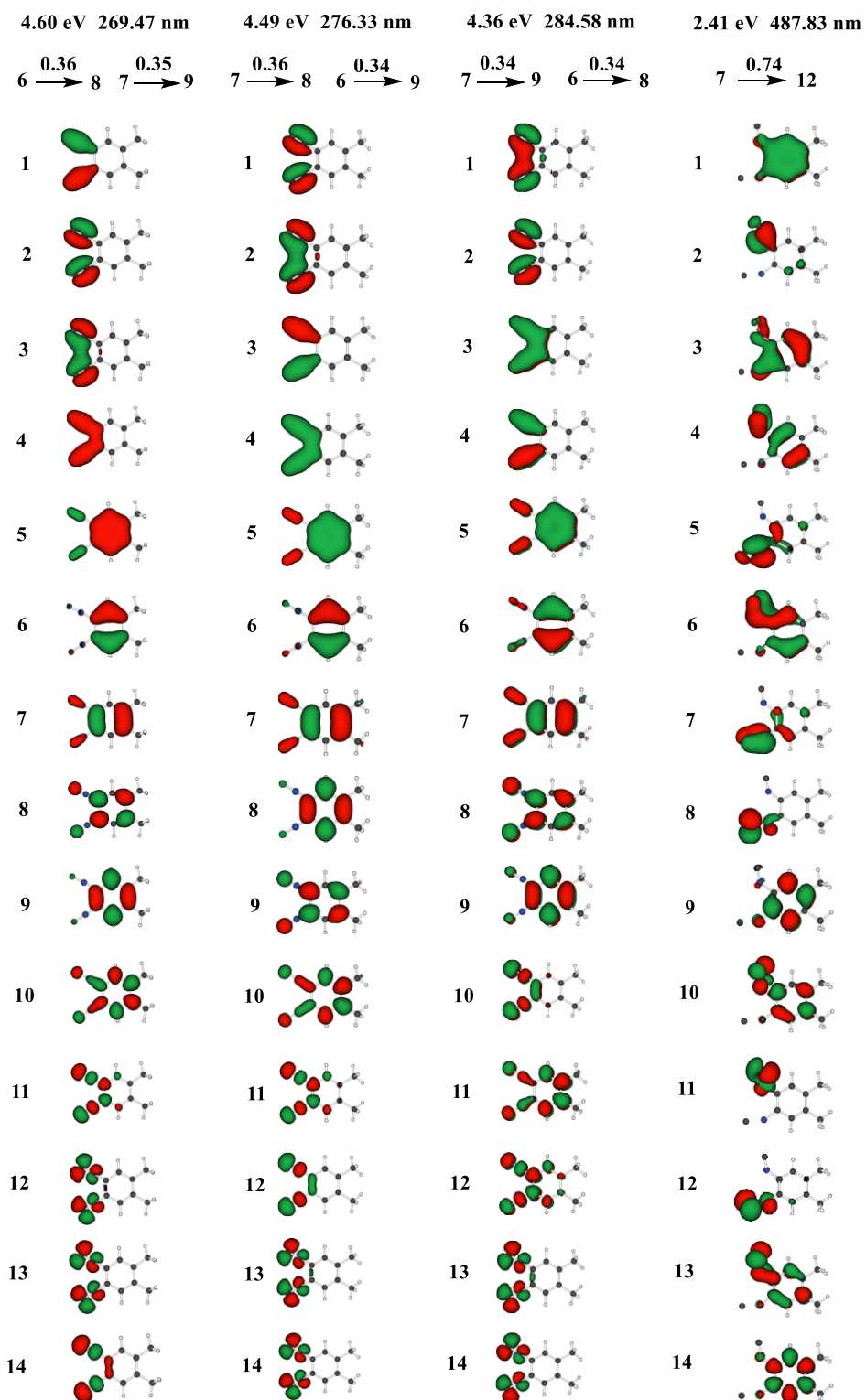


**Figure S2.** The 14 active orbitals and excitation configurations for  $S_1$  of 4 isomers with different geometries.

According to **Table S2** and **Figure S3**, the lowest singlet excited states  $S_1$  of (1-1), (1-

**2)** and **(1-3)** are similar: the excitation configurations are involved with  $\pi$  orbitals to  $\pi^*$  orbitals of the whole conjugation system. As the C-N distance ( $r_{\text{C-N}}$ ) increases, the gap between  $\pi$  orbital of C-N and  $\pi^*$  orbital of C-N decreases. As a result,  $\pi$  orbitals of C-N to  $\pi^*$  orbitals of C-N excitation configurations give dominant weights in **1-iso** for low-lying singlet excited states.

In addition, **Table S3** lists results of excited energies of CASSCF and CASPT2 calculations. And the results of CASSCF oscillator strengths  $f$  of low-lying singlet excited states are also displayed in **Table S3**.

### 3.3. CASSCF/CASPT2 results: excitation energies and oscillator strengths $f$

**Table S3-a: Low-lying excitation energies (eV) obtained by CASSCF/CASPT2 <sup>a</sup>**

state	(1-1)	(1-2)	(1-3)	(1-iso)
S <sub>1</sub>	4.60/4.70	4.49	4.36	2.41/2.65
S <sub>2</sub>	7.12/5.76	6.96	6.59	3.06/3.28
S <sub>3</sub>	7.57/6.41	7.44	7.17	-
S <sub>4</sub>	7.74/7.57	7.48	7.23	-

**Table S3-b: Oscillator strengths  $f$  of the studied systems**

state	(1-1)	(1-2)	(1-3)	(1-iso)
S <sub>1</sub>	<b>0.00</b>	<b>0.00</b>	<b>0.00</b>	<b><math>2.9 \times 10^{-3}</math></b>
S <sub>2</sub>	<b><math>1.1 \times 10^{-1}</math></b>	<b><math>1.2 \times 10^{-1}</math></b>	<b><math>1.7 \times 10^{-1}</math></b>	<b><math>3.4 \times 10^{-3}</math></b>
S <sub>3</sub>	<b><math>1.1 \times 10^{-2}</math></b>	<b><math>4.2 \times 10^{-2}</math></b>	<b><math>1.3 \times 10^{-1}</math></b>	-
S <sub>4</sub>	<b><math>3.1 \times 10^{-2}</math></b>	<b><math>9.1 \times 10^{-2}</math></b>	<b><math>8.3 \times 10^{-2}</math></b>	-

<sup>a</sup> CASPT2 calculation was applied for (1-1) and (1-iso) only.

#### 4. Comparison between experiment and DFT calculation: IR spectra and forms of NC bending modes for 1-S<sub>0</sub>, 1-S<sub>1</sub>, 1-T<sub>1</sub>.

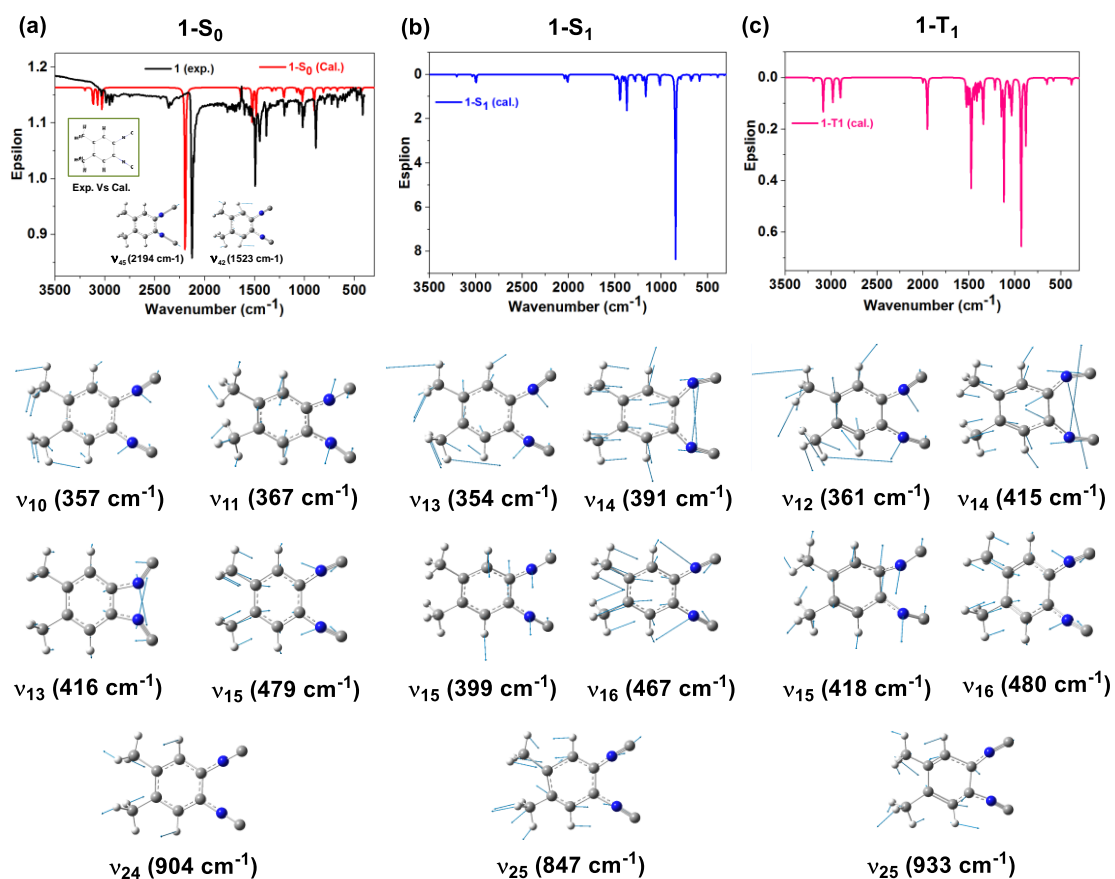


**Figure S3.** The IR spectra of experimental (black line) and the calculated results (red line) obtained at B3LYP/6-311+G(d, p) and forms of NC bending modes for 1-S<sub>0</sub>, 1-S<sub>1</sub>, 1-T<sub>1</sub>

## 5. Binding energies of $\pi$ - $\pi$ stacking configuration in crystal

**Table S4.** The binding energies of  $\pi$ - $\pi$  stacking configuration (n=4) with different calculation levels.

calculation levels	Monomer (Hartree)	$\pi$ - $\pi$ stacking configuration (Hartree)	$E_b$ (eV)
crystal	-495.133504	-1980.612709 (n = 4)	-2.14 <sup>a</sup>
PW91/DND4.4	-495.268909	-1981.150843 (n = 4)	-2.04
PW91-D/DND4.4	-495.301629	-1981.4928159 (n= 4)	-7.79
B3LYP/b1 <sup>b</sup>	-495.309521	-1981.225227 (n = 4)	0.35
M06-2X/ b1 <sup>b</sup>	-495.108327	-1980.474561 (n = 4)	-1.12
CAM-B3LYP/b1 <sup>b</sup>	-495.038910	-1980.156638 (n = 4)	-0.03
B97-2/ b2 <sup>c</sup>	-495.178912	-1980.699229 (n = 4)	0.45

<sup>a</sup>GGA/PW91/DND4.4

<sup>b</sup>basis set b1: 6-311+G(d,p)

<sup>c</sup>basis set b2: def2TZVP

## 6. Experimental and calculated values for $S_0 \rightarrow S_1$ transitions

Table S5. The  $S_0 \rightarrow S_1$  transitions for the studied systems in gas phase

molecule	$S_0 \rightarrow S_1$ gas-phase		
	exp. (nm)	cal. (nm) <sup>b</sup>	cal. (nm) <sup>c/f</sup>
<b>1</b>	<b>260</b> <sup>c</sup>	<b>268</b>	<b>259/0.26</b>
<b>4</b>	-	<b>275</b>	<b>268/0.15</b>
<b>5</b>	<b>285</b> <sup>a</sup>	<b>275</b>	<b>262/0.04</b>
<b>6</b>	<b>281</b> <sup>a</sup>	<b>269</b>	<b>255/0.01</b>

<sup>a</sup> Mehta-Hurt, D. N.; Korn, J. A.; Gutberlet, A. K.; Zwieter, T. S. *J. Phys. Chem. A* **2015**, 119, 2863–2877. <sup>b</sup> TD-DFT results from *J. Phys. Chem. A* **2015**, 119, 2863–2877. Optimization calculations were run at the level of B3LYP/6-31+G(d). <sup>c</sup> TD-DFT calculations done in this work at the level of B3LYP/6-311+G(d,p).

To investigate the role of isocyanides in chemical processes in Titan's atmosphere, Zwieter and co-workers carried out vibronic spectroscopy study of disubstitutedcyano/isocyno derivatives, dicyanobenzene (DCB, **5**) and *para*-diisocyanobenzene (*p*DIB, also called DiCNB, **6**) under jet-cooled conditions in the gas phase.<sup>19</sup> The experimental  $S_0$ - $S_1$  excitation energies (**5**: 285 nm; **6**: 281 nm) in gas phase are close to the calculated values of **1** and **4** with two additional methyl groups attaching on the aromatic ring. The good agreement in the lowest vertical transition energies of **5** and **6** between the experimental observations in gas phase and TDDFT calculations on the isolated molecule was demonstrated in both recent publication<sup>19</sup> and this work (Table S5).

## 7. The electrostatic potential and monomer charge of $\pi$ - $\pi$ stacking configuration

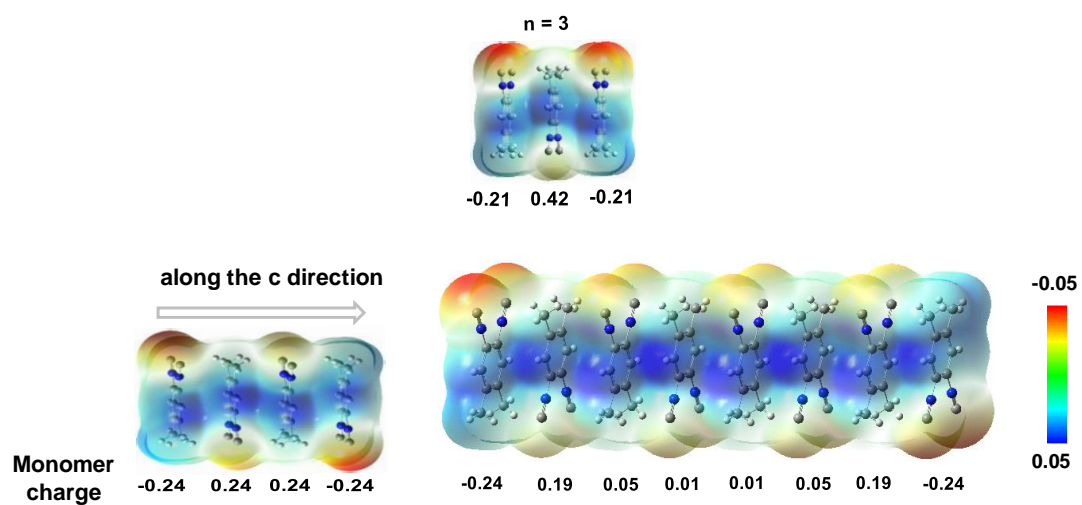
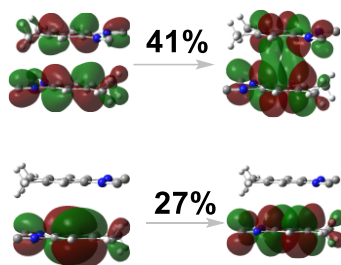


**Figure S4.** The electrostatic potential and monomer charge of  $\pi$ - $\pi$  stacking configurations ( $n = 3, 4, 8$ ).

## 8. Natural transition orbitals of $S_0 \rightarrow S_1$ transition for oligomers.

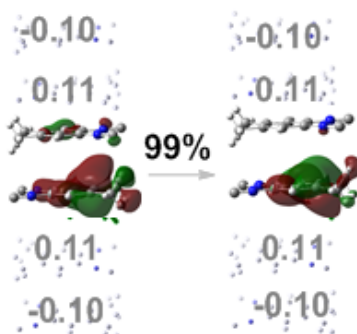
$S_0 \rightarrow S_1$  ( $n = 2$ )  
Natural transition orbitals



(a) Dimer

$S_0 \rightarrow S_1$

Natural transition orbitals



(b) Dimer@BG

**Figure S5.** Natural transition orbitals for  $S_0 \rightarrow S_1$  when (a)  $n = 2$  and (b) a dimer is embedded in background point charges (BG), the percentage is the weight of  $S_0 \rightarrow S_1$  transition density, predicted at the level of M06-2X/6-311+G(d,p).

## 9. Computational results using different DFT functionals

**Table S6-a.** Comparison of DFT Functionals Used in This Work.

functional	percentage of HF exchange in the functional
B3LYP	20%
M06-2X	54%
B97-2	21%
$\omega$ B97X-D	short range 22.2%, long range 100%, $\omega=0.2$
CAM-B3LYP	short range 19%, long range 65%, $\omega=0.33$

**Table S6-b.** TD-DFT Singlet Transition Energies ( $E_{\text{ex}}$ ) and Oscillator Strengths ( $f$ ) for **1** in Gas-phase, X-Ray Geometries, and Solvation Structures by Using Different DFT Functionals (with the background charges representing the electrostatics environment).

	functional	$E_{\text{ex}}$ (nm)	$f$	Transition weights <sup>a</sup>		note
				configuration	coefficients	
Gas-phase	B3LYP (monomer)	259	0.26	H→L	0.95	Fig. S6
	CAM-B3LYP (monomer)	240	0.27	H→L+1	0.54	
	M06-2X (monomer)	236	0.27	H→L	0.92	Fig. 1E
crystal oligomer@BG (n=3)	B3LYP	486	0.03	H-4→L+2	0.61	Fig. S6
	M06-2X	513	0.07	H-2→L+1	0.46	Fig. 1E
		486	0.07			
Crystal oligomer@BG (n=6)	B3LYP	484	0.03	H-2→L+6	0.72	Fig. S6
	M06-2X	507	0.02	H-3→L+3	0.41	Fig. 1E
		468	0.03			
Crystal with or w/o BG	$\omega$ B97X-D (dimer)	234	0.39	H→L+1	0.54	
crystal with or w/o BG	CAM-B3LYP (dimer)	235	0.38	H→L+1	0.55	

amorphous from AIMD	M06-2X (6.5 ps)	522,467	0.015,0.012		
	M06-2X (7.0 ps)	517,467	0.013,0.012		
	M06-2X (9.0 ps)	273,264	0,012,0.266		
	M06-2X (10.0 ps)	274,262	0.009,0.371		
solvation@CH <sub>3</sub> CN from AIMD	M06-2X (12 ps)	541,463	0.013,0.011		
	M06-2X (15 ps)	502,468	0.042,0.046		
	M06-2X (18 ps)	403,389	0,010,0.012		
	M06-2X (21 ps)	598,469	0.015,0.058		
	M06-2X (24 ps)	574,443	0.013,0.016		
	M06-2X (27 ps)	429,421	0.052,0.074		
	M06-2X (33 ps)	624,429	0.019,0.052		
	M06-2X (36 ps)	537,454	0.024,0.076		
solvation@ CH <sub>3</sub> CN	$\omega$ B97X-D (explicit model: <b>1</b> @10 CH <sub>3</sub> CN)	235	0.18	H→L	0.64
	$\omega$ B97X-D ( <b>1</b> @BG model)	233	0.23	H→L	0.67
solvation@ CH <sub>3</sub> CN	CAM-B3LYP (explicit model: <b>1</b> @10 CH <sub>3</sub> CN)	236	0.18	H→L	0.64
	CAM-B3LYP ( <b>1</b> @BG model)	234	0.23	H→L	0.66
+e/-e embedding (3.5Å)	CAM-B3LYP (dimer)	511	0.02	H→L+3	0.63
		497	0.02	H→L+4	0.55
+e/-e embedding (4.5Å)	CAM-B3LYP (dimer)	525	0.05	H→L+1	0.69
		516	0.06	H→L+2	0.70
		500	0.08	H→L+3	0.70

<sup>a</sup> Transition weights denote dominant configuration (HOMO=H, LUMO=L) and their coefficients.

The low-lying excited states of **1** were calculated using TDDFT with B3LYP, M06-2X, and range-separated hybrid CAM-B3LYP and  $\omega$ B97X-D functionals, respectively. For an isolated molecule (also called monomer), the choice of different DFT functionals gives the similar TDDFT calculation values of  $\lambda_{\max}$  in the absorption of about 259 nm (with B3LYP functional), 236 nm (M06-2X), 240 nm (CAM-B3LYP) and 255 nm (B97-2), respectively. The wavelengths and relative energies under different calculation levels are shown in Figure S1. The CASSCF/CASPT2 calculations with 14 active electrons in 14 active orbitals also predict similar UV absorption at around 270 nm with the optimized gaseous geometry.

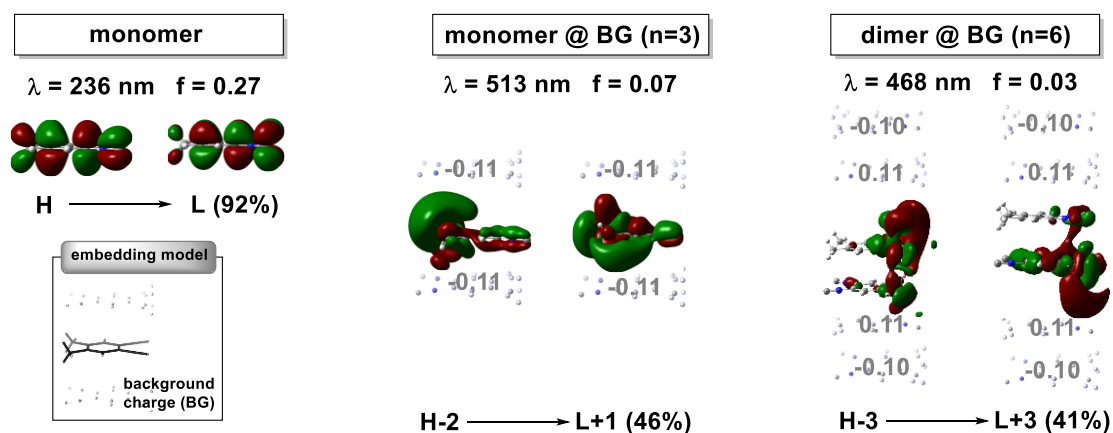
To better understand the  $\pi$  stacking effects on absorption spectrum of **1** in solid state, the electrostatic embedding model is introduced to demonstrate the red shift of  $\lambda_{\max}$  from UV (for an isolated monomer) to visible-light scope using M06-2X (Figure 1E) and B3LYP (Figure S6), respectively. Table S6 collects all the computational results of excitation energies and oscillator strengths with M06-2X, B3LYP, CAM-B3LYP, S16

$\omega$ B97X-D functionals. When the monomer **1** is embedded in atmosphere of background point charges (BG), which were obtained from DFT calculations on  $n = 3$  stacking array with the induced fragment charge of about  $-\rho \approx 0.21$ . The usage of M06-2X and B3LYP functionals in the electrostatics embedding model led to similar results, so we present the M06-2X results in text and the B3LYP data in supporting information. However, the CAM-B3LYP and  $\omega$ B97X-D functionals are not sensitive to the introduction of the background charges of the adjacent molecules in TDDFT calculations (Table S6). However, the CAM-B3LYP and  $\omega$ B97X-D functionals are not sensitive to the introduction of the background charges of the adjacent molecules in TDDFT calculations (Table S6). With or without the introduction of BG charges, TDDFT computations with the CAM-B3LYP and  $\omega$ B97X-D functionals gave nearly identical results. Only for the highly polarized system with the background charges of +1 and -1 putting on the top and bottom of the dimer, the CAM-B3LYP and  $\omega$ B97X-D excitation energies are red-shifted to the visible region (c.f., the last two lines in Table S6). For  $\pi$  stacking systems, future works are still required to find suitable methods to reproduce the experimental spectra of charge transfer excitation in visible light region.

In our AIMD simulations of solvated **1** in both CH<sub>3</sub>CN and Et<sub>2</sub>O solvent molecules, the energetically higher conformation occurs with the distorted geometry and lengthened N-C bonds in isocyano groups, probably due to the disturbance of the solvent molecules in thermal motions under room temperature. Those distorted structures also lead to the visible-light absorption ability of **1** (Figure S8). In addition, the resonance forms of **1** (with higher energetic carbene character) are also able to cause a red shift in maximum absorption according to CASPT2/CASSCF calculations, as shown in Figure S1 and Table S3. For the aggregation induced symmetry-broken geometries (taken from AIMD simulations), all the selected DFT functionals (including B3LYP, M06-2X, CAM-B3LYP, and  $\omega$ B97X-D) gave similar TDDFT results.

## 10. TDDFT calculations on $\pi$ stacking arrays with background charges

(a) M06-2X/6-311+G(d, p)



(b) B3LYP/6-311+G(d, p)

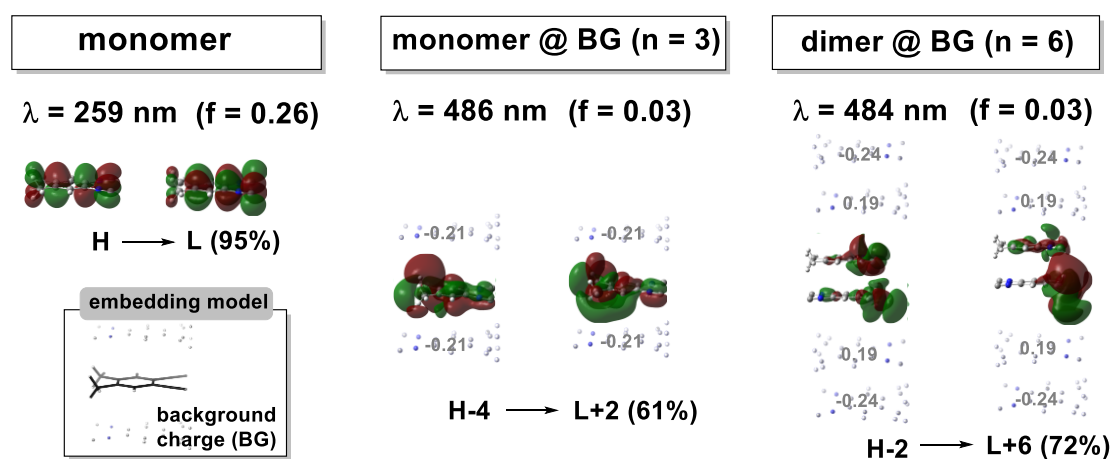


**Figure S6.** The DFT calculations on  $n = 3$  and  $6$  stacking arrays with the induced fragment charges. At the B3LYP/6-311+G(d,p) level, the corresponding maximum absorption wavelength is about  $486 \text{ nm}$  with the weak oscillator strength ( $f$ ) of  $0.03$ .

11. Experimental absorption spectra of unitary, binary and trinary mixtures 1, 2, Bn<sub>2</sub>NH in CH<sub>3</sub>CN solvent

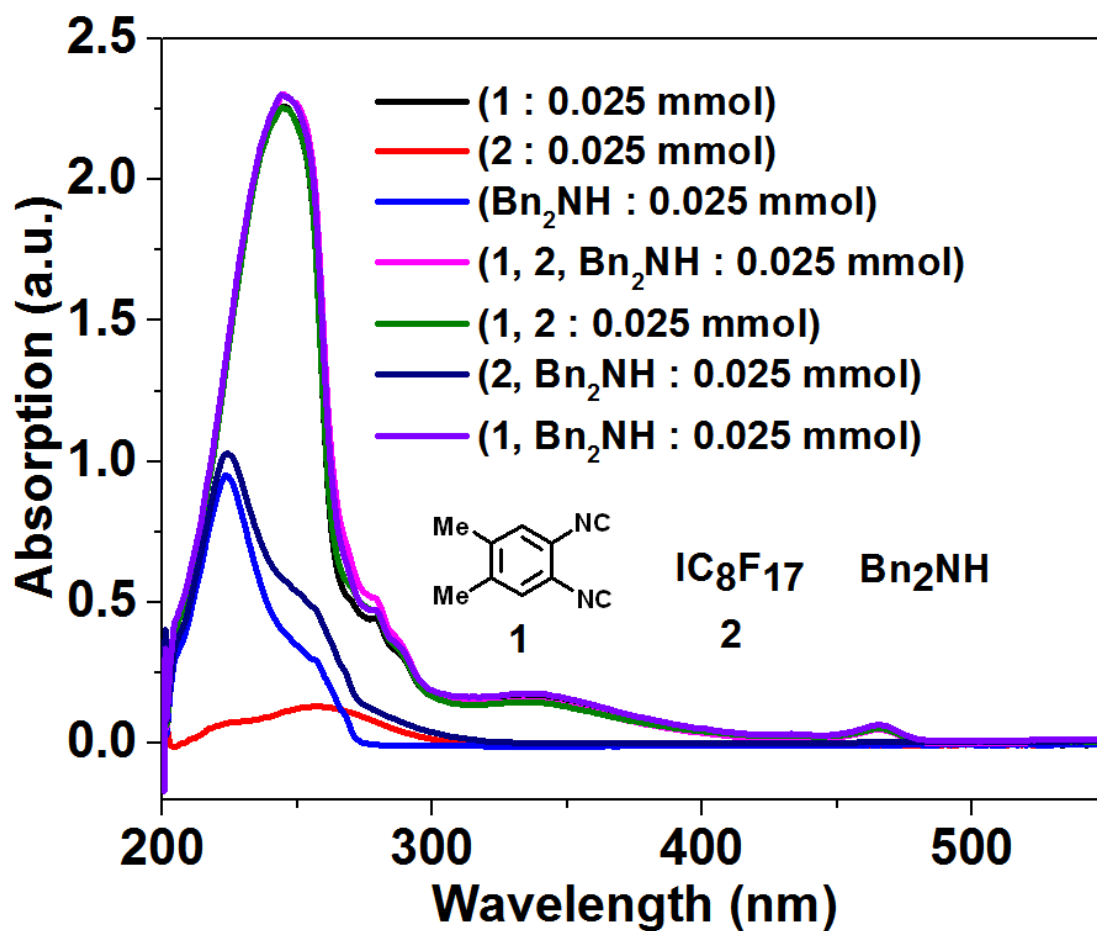
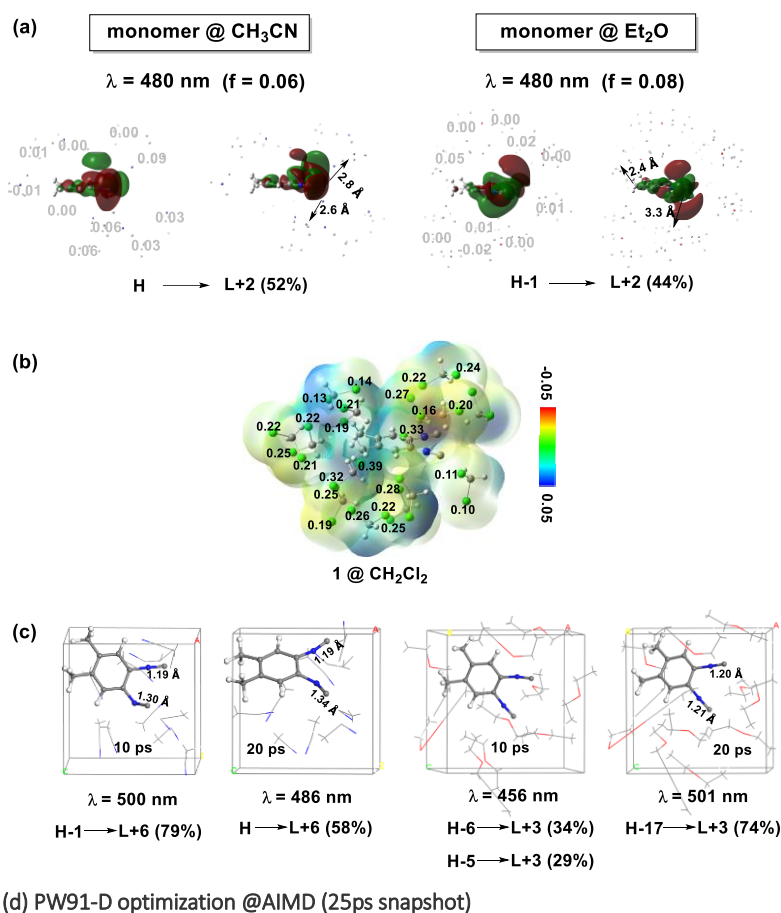


Figure S7. The absorption spectra of 1, 2, Bn<sub>2</sub>NH and their mixtures in CH<sub>3</sub>CN solvent.

## 12. TDDFT calculation results of monomer @ CH<sub>3</sub>CN and monomer @ Et<sub>2</sub>O solvent and AIMD simulations of solvated 1 in both CH<sub>3</sub>CN and Et<sub>2</sub>O solvent molecules



**Figure S8.** (a) TDDFT calculation results using B3LYP/6-311+G(d, p) of absorption wavelengths and oscillator strengths along with transition orbitals of monomer @ CH<sub>3</sub>CN and monomer @ Et<sub>2</sub>O solvent. (b) The electrostatic potential of 1 @ CH<sub>2</sub>Cl<sub>2</sub>. (c) AIMD simulations of solvated 1 in both CH<sub>3</sub>CN and Et<sub>2</sub>O solvent molecules and the distorted structures also lead to the visible-light absorption ability of 1. (d) Dipole-dipole interactions between solvent molecules and solutes in PW91-D optimized solvation structures based on AIMD snapshots at 25 ps.

### 13. The experimental absorption spectra of 1 in other solvents

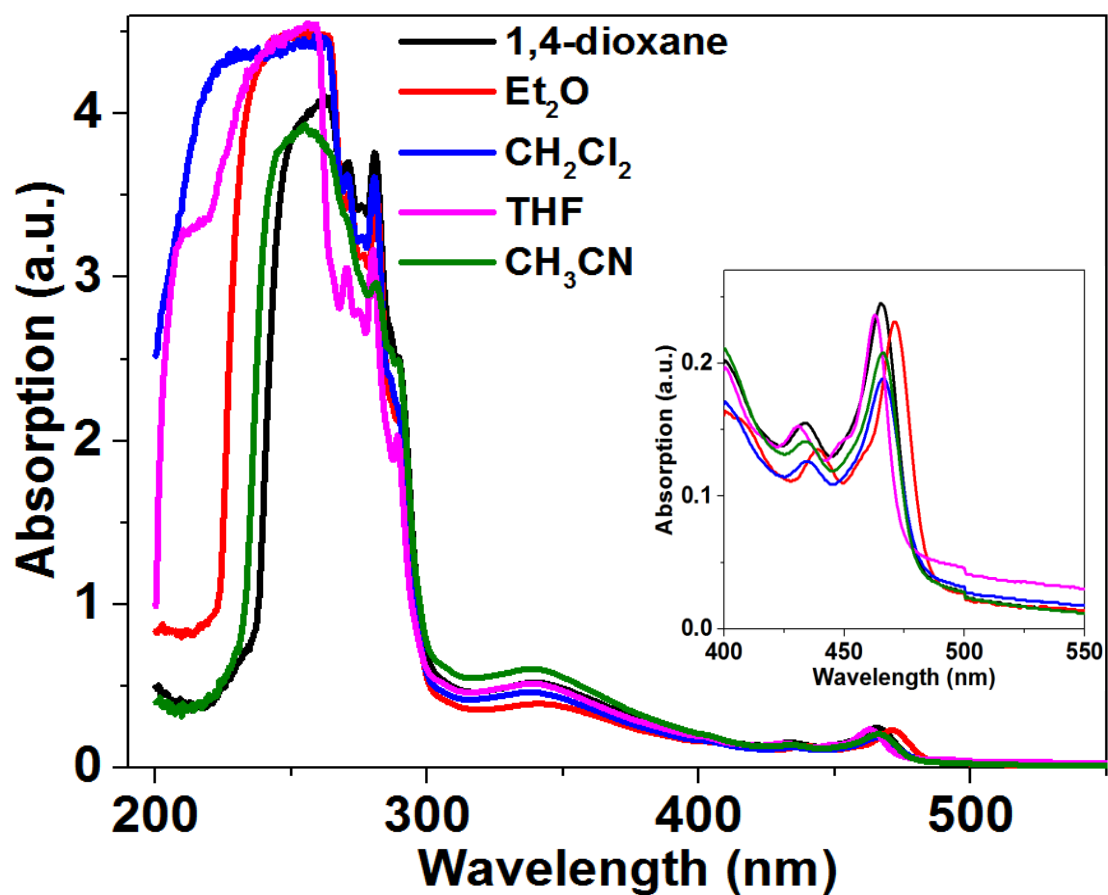
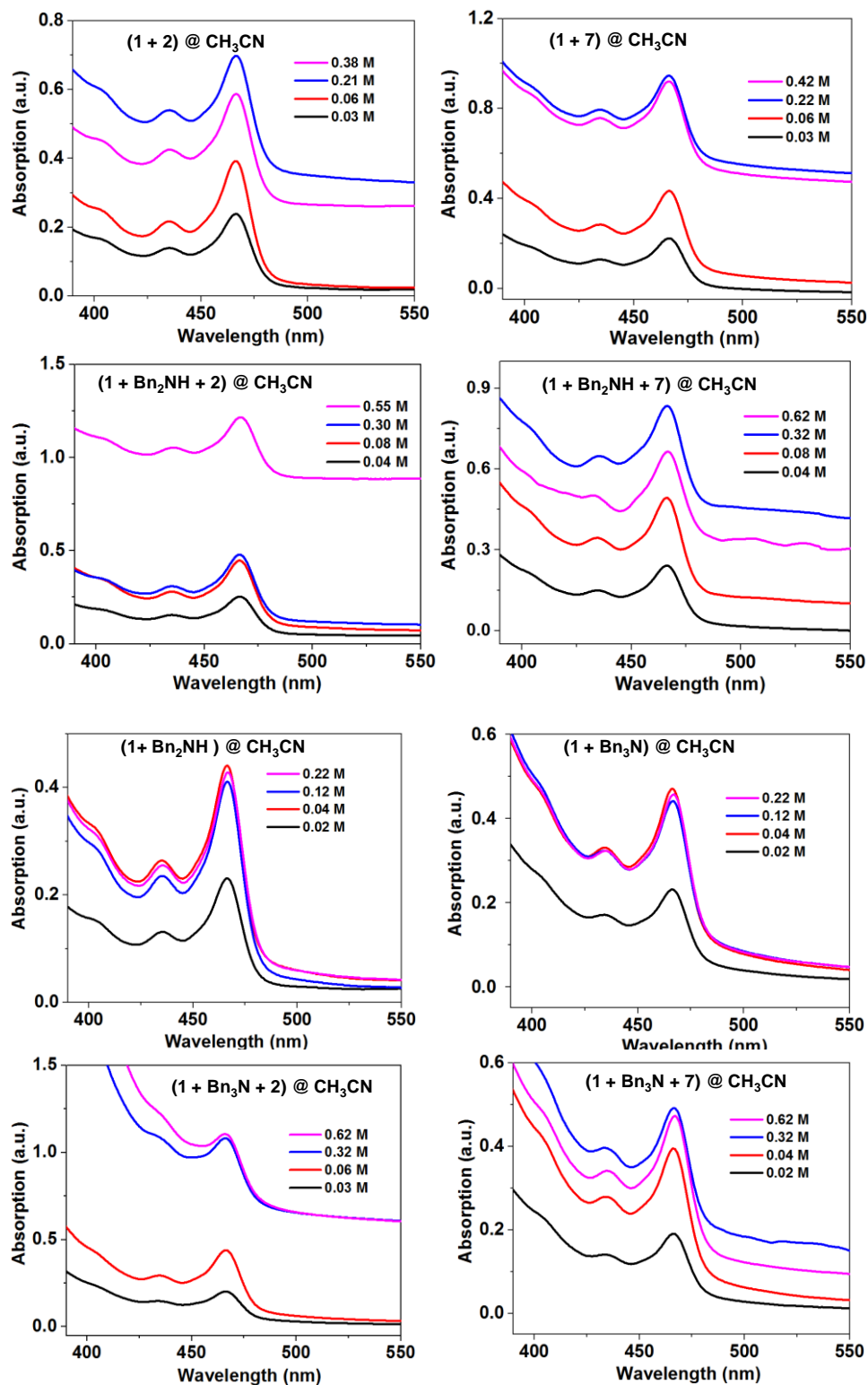


Figure S9. The experimental absorption spectrum of 1 in various solvents (CH<sub>3</sub>CN, 1,4-dioxane, THF, Et<sub>2</sub>O, CH<sub>2</sub>Cl<sub>2</sub>).

14. The absorption spectra of binary and ternary mixtures of 1, 2 (7), and  $\text{Bn}_2\text{NH}$  ( $\text{Bn}_3\text{N}$ ) in  $\text{CH}_3\text{CN}$  solvent.



**Figure S10.** The absorption spectra of binary and ternary mixtures of 1, 2 (7), and  $\text{Bn}_2\text{NH}$  ( $\text{Bn}_3\text{N}$ ) in  $\text{CH}_3\text{CN}$  solvent.

### 15. TDDFT and experimental absorption spectra of product 3

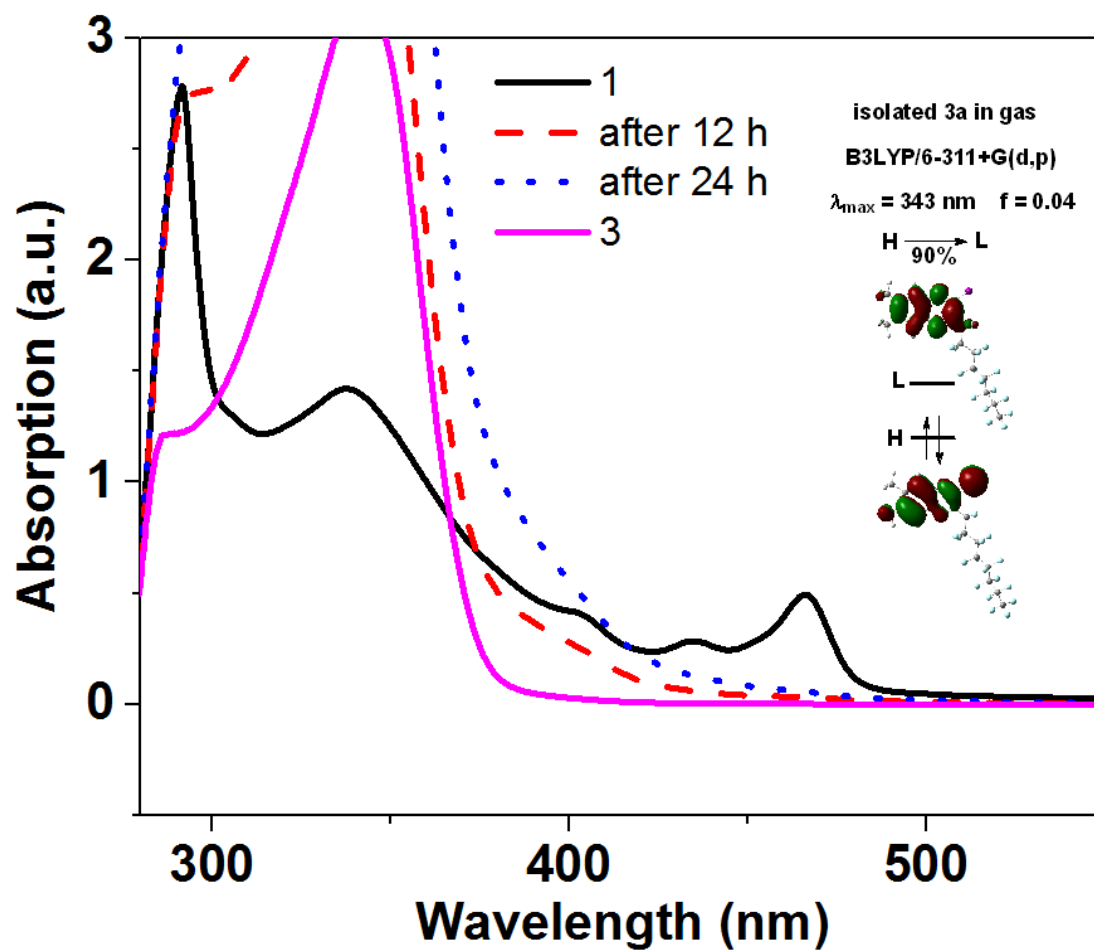
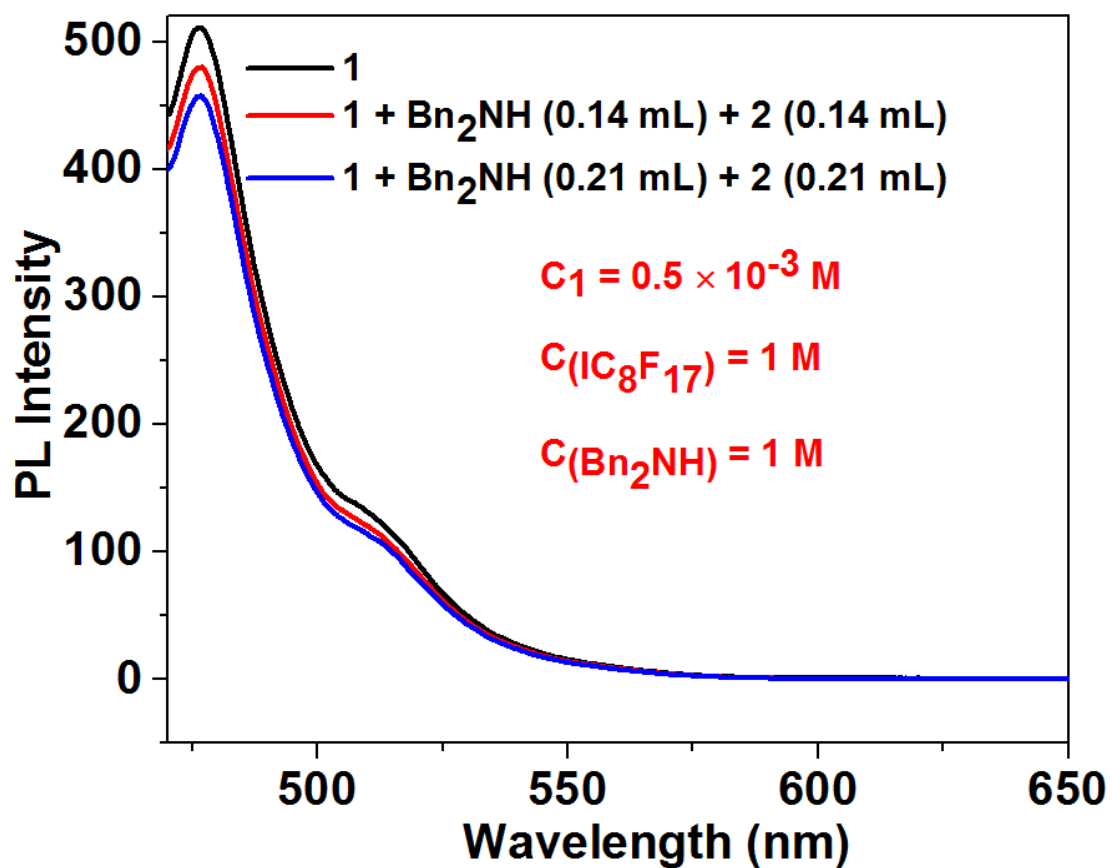


Figure S11. TDDFT predicted and experimental UV-vis spectrum of product 3.

## 16. The fluorescence quenching of the mixture of 1, 2 and Bn<sub>2</sub>NH



**Figure S12.** The fluorescence quenching of the mixture of 1, 2 and Bn<sub>2</sub>NH with the concentration (c) of 1 is 0.5 mM.

## 17. The frontier molecular orbitals of donors and acceptors in reactions

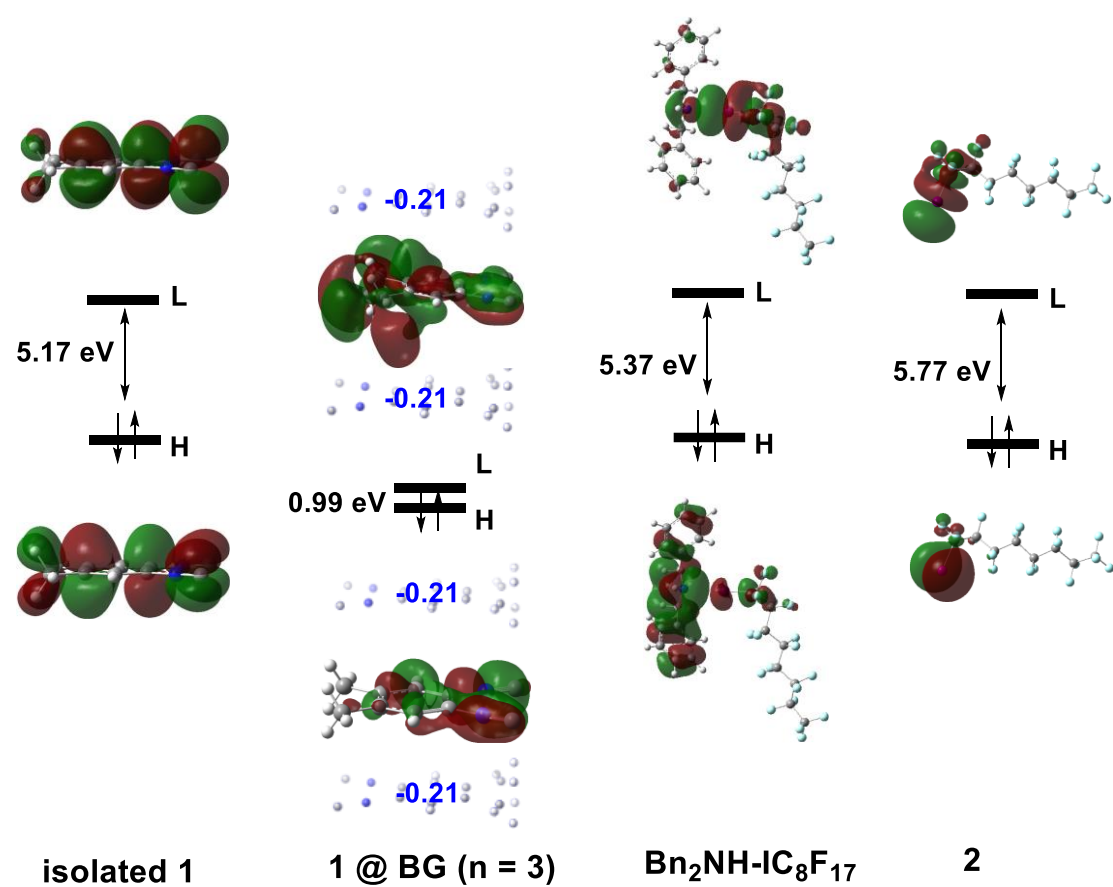


**Figure S13.** The frontier molecular orbitals of 1 or 1 embedded in atmosphere of BG (n = 3) is as donor and 2 or Bn<sub>2</sub>NH-IC<sub>8</sub>F<sub>17</sub> is as acceptor.

## 18. The absorption wavelengths and oscillator strengths of the isolated **4** and embedded **4 @ BG (n = 3)**

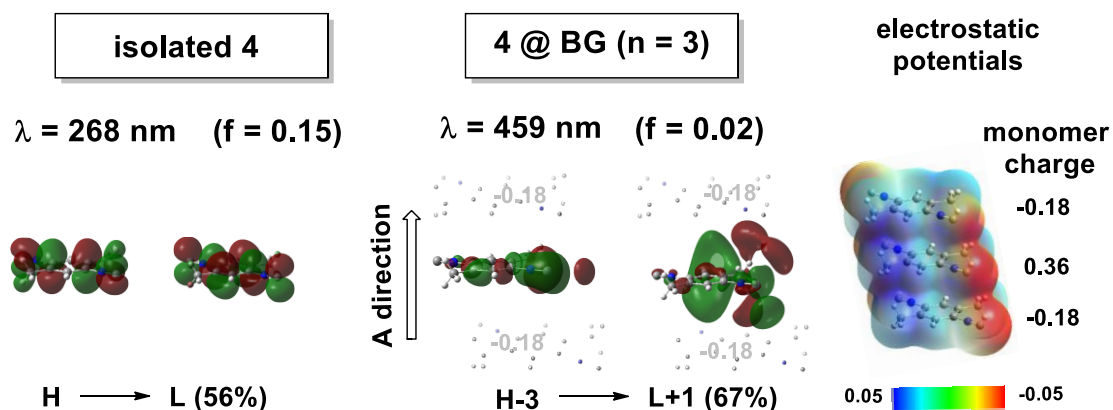


**Figure S14.** The absorption wavelengths and oscillator strengths along with orbitals of the isolated **4** and embedded **4 @ BG (n = 3)** aggregate, the electrostatic potential and monomer charge of **4** in  $\pi$ - $\pi$  stacking configurations ( $n = 3$ ) with B3LYP/6-311+G(d, p).